A Joint-Constraint Model-Based System for Reconstructing Total Knee Motion

Hsin-Chen Chen, Chia-Hsing Wu, Chien-Kuo Wang, Chii-Jeng Lin, and Yung-Nien Sun*, *Senior Member, IEEE*

***Abstract*—Comprehending knee motion is an essential requirement for studying the causes of knee disorders. In this paper, we propose a new 2-D–3-D registration system based on joint-constraint model for reconstructing total knee motion. The proposed model that contains bone geometries and an articulated joint mechanism is first constructed from multipostural magnetic resonancevolumetric images. Then, the bone segments of the model are hierarchically registered to each frame of the given single-plane fluoroscopic video that records the knee activity. The bone posture is iteratively optimized using a modified chamfer matching algorithm to yield the simulated radiograph which is the best fit to the underlying fluoroscopic image. Unlike conventional registration methods computing posture parameters for each bone independently, the proposed femorotibial and patellofemoral joint models properly maintain the articulations between femur, tibia, and patella during the registration processes. As a result, we can obtain a sequence of registered knee postures showing smooth and reasonable physiologic patterns of motion. The proposed system also provides joint-space interpolation to densely generate intermediate postures for motion animation. The effectiveness of the proposed method was validated by computer simulation, animal cadaver, and *in vivo* knee testing. The mean target registration errors for femur, tibia, and patella were less than 1.5 mm. In particular, small out-of-plane registration errors [less than 1 mm (translation) and 2° (rotation)] were achieved in animal cadaver assessments.**

***Index Terms*—2-D–3-D registration, joint-constraint model, knee motion reconstruction, magnetic resonance (MR), single-plane fluoroscopy.**

I. Introduction

THE knee is the largest and the most complex joint structure in the human body. It plays an essential role in human motion, and unfortunately, long-term usage and injuries tend to lead to the degeneration of knee joint functions. Moreover, knee osteoarthritis has been reported as the most common chronic joint disorder in elderly people, and is a disabling disease with many individual risk factors that might affect the quality of life [1]. The correlation of these factors with the structural progression of osteoarthritis has been mostly investigated based on radiographic evaluations. However, such 2-D analyses may not be able to provide enough evidences in clinical diagnosis for good outcome of medical intervention [2]. In general, knee degeneration can be evaluated based on several parameters, e.g., load distribution, contact area, and ligament tension during knee motion. To measure these parameters and learn better the pathomechanism, reconstructing 3-D knee kinematics is hence rather important. This paper aims to explore and develop an image analysis system for noninvasively and automatically reconstructing total knee motion.

Most previous research has focused on analyzing knee kinematics, primarily derived from data attained through skin markers tracked using a motion capture system. Chen *et al*. [3] and Lin *et al*. [4] utilized a 3-D knee surface model and moving marker data to simulate and visualize knee motion. Lin *et al*. [5] employed an optoelectronic marker tracking system to investigate patella behavior during knee flexion and extension. Although the use of a motion capture system permits easy collection of knee motion data, the accuracy of marker tracking may potentially decrease due to the deformation of soft tissues (e.g., skin movement or muscle contraction), making the reconstructed knee motion prone to biases [6].

To overcome this drawback, image-based motion analysis methods have been considered. Over recent years, there has been a rapid development of noninvasive imaging devices for visualizing the geometries of human internal structures. For example, single-plane fluoroscopy can be used to acquire a sequence of projection images that records the posture changes of imaged object during activity. Computer tomography (CT) and magnetic resonance (MR) scanners mostly provide high-quality volumetric images for static postures. Although CT imaging can produce very high-quality images for bony structures, it results in the irradiation of study volunteers in each acquisition. As to MR scanning, it can also provide reasonably clear boundaries of bony structures, and more importantly, is radiation free. Another potential merit is that it enables the visualization of anatomical details of soft tissues, which is unavailable in CT imaging. Considering that the knee joint contains both rigid bones and soft tissues, using MR modality can preserve better extensibility of the system to include soft tissues, e.g., patella ligament and anterior cruciate ligament, for investigating more complete knee

Manuscript received February 3, 2013; revised July 7, 2013; accepted August 8, 2013. Date of publication August 15, 2013; date of current version December 16, 2013. This work was supported by the grant from the National Science Council, Taiwan, under Contract NSC 101-2221-E-006–059-MY3, Also, this work made use of shared facilities supported by the Program of Top 100 Universities Advancement, Ministry of Education, Taiwan. *Asterisk indicates corresponding author*.

H.-C. Chen is with the Department of Neurological Surgery, University of Pittsburgh, PA 15213 USA (e-mail: hsinlovehsin@gmail.com).

C.-H. Wu is with the MPI Corporation, Hsinchu County 302, Taiwan (e-mail: btmage@gmail.com).

C.-K. Wang is with the Department of Radiology, National Cheng Kung University Hospital, Tainan 70101, Taiwan (e-mail: n044206@mail.hosp.ncku.edu.tw).

C.-J. Lin is with the Department of Orthopedics, National Cheng Kung University, Tainan 70101, Taiwan (e-mail: mark@mail.ncku.edu.tw).

*Y.-N. Sun is with the Department of Computer Science and Information Engineering, National Cheng Kung University, Tainan 70101, Taiwan (e-mail: ynsun@mail.ncku.edu.tw).

Color versions of one or more of the figures in this paper are available online at http://ieeexplore.ieee.org.

Digital Object Identifier 10.1109/TBME.2013.2278780

motion. Thus, MR and single-plane fluoroscopy were selected as the image modalities for knee motion reconstruction in this study.

2-D–3-D image registration is the process of identifying an optimal 3-D geometric transformation which can sufficiently match a 3-D object to a specific projection image. In the early days, Banks *et al*. [7] and Zuffi *et al*. [8] proposed using 2-D–3-D registration to noninvasively measure the dynamic femorotibial contact of knee implants of patients with total knee arthroplasty. Their registration systems were designed for the fluoroscopic images of metallic components, which present a large degree of homogeneous intensity and sharp boundaries. Nevertheless, they did not overcome the drawbacks caused by inherent artifacts of X-ray imaging on natural knee joints, e.g., unevenly distributed intensity in knee bone regions and fuzzy bone boundaries. These drawbacks make it difficult to extract the complete borders of bone segments from fluoroscopic images, thus leading to the instability of feature matching during the registration process.

Some studies have attempted to improve the fitness measures of 2-D–3-D registration to better accommodate the drawbacks of X-ray imaging. Fregly *et al*. [9] and Tsai *et al*. [10] proposed using contour-based measures to register knee bone surface models to fluoroscopic images. Penney *et al*. [11] presented a validation of intensity- and gradient-based 2-D–3-D registration algorithms. Ma *et al*. [12] proposed a template matching-based method with a normalized correlation coefficient for registration of multiple bones. Although these methods achieved good registration by exploring different image features, they were unable to handle the insufficiencies occurring in spatial information in single-plane fluoroscopic images. This difficulty is because slight object translations perpendicular to the projection image plane do not result in obvious changes to the projection details [13]. The bone registration, which only utilizes image features without taking the articulation of the knee joint into account, is prone to be trapped by incorrect local solutions, especially in the case of out-of-plane motion (i.e., motion along the projection direction). More specifically, two articulated bone segments may be dislocated if they are registered independently; significant differences which violate the joint constraint may appear in the registration results.

Although it has been reported that patellofemoral pain syndrome (e.g., runner's knee) is a common musculoskeletal condition in young people [14], [15], existing 2-D–3-D registration systems for natural knees mainly have addressed the issue of reconstructing the kinematics of the femur and tibia. Only rare studies have developed image-based approaches for reconstructing patella motion [16]. The patella has a smooth shape and is relatively small as compared to the femur and tibia, so accountable image and shape features for 2-D–3-D registration are very limited. Again, without incorporating additional domain knowledge such as knee anatomy and biomechanics, accurate registration for the total knee (femur, tibia, fibula, and patella) is hard to achieve.

Beyond that, there is another unresolved issue in reconstructing total knee motion (i.e., femur, tibia, fibula, and patella). The knee bone segments can afford a wide range of motion, so large postural differences between a 3-D knee model and 2-D fluoroscopic images are very like to occur. It is difficult to automatically place each bone segment of the knee model close to the corresponding position on each image. Therefore, manually initializing proper knee posture remains the most common method by which to do this [9], but it is, however, tedious, time-consuming, and operator-dependent.

In our previous study, we proposed using an articulated hand model to segment hand bones from multipostural MR images [17]. It was found that using an anatomical model with proper kinematic properties and image features can efficiently resolve the variations among the contents of different images as well as those occurring in conjunction with object motion. Adding to this, in this paper, we propose a new model-based image registration system for reconstructing total knee motion. For each subject, given the multipostural MR images to construct a knee model, the proposed method can automatically reconstruct his/her knee motion using the proposed registration method with single-plane fluoroscopy.

Major improvements involved in the proposed method, as compared to conventional methods, are described next. The proposed knee model, characterized by an articulated joint mechanism intended to constrain knee motion, can compensate for the insufficiency of spatial information in single-plane fluoroscopic images. Moreover, the proposed method can automatically drive each bone of the knee joint to a good initial condition for facilitating convergence of registration as well as for reducing the time cost of manual adjustments. We also design a noncorresponding point removal scheme to achieve better matching between 2-D and 3-D image features. More importantly, the proposed joint-constraint model covers both femorotibial and patellofemoral joints, thus enabling investigation of total knee motion. Overall, our proposed method can cope with the aforementioned difficulties in 2-D–3-D knee image registration. This paper is arranged as follows. Section II gives the details of the proposed method, Sections III and IV describes the experimental results and discussions, respectively, and the final section provides the conclusion.

II. Method

A. Overview of the Proposed System

To reconstruct 3-D knee motion using single-plane fluoroscopy, we first require the derivations of the projection parameters of fluoroscopy. Then, a knee model consisting of bone geometries and an articulated joint mechanism is constructed from multipostural MR images. We then apply the projection parameters and knee model to the model-based registration stage. The bone segments of the knee model are hierarchically registered to the fluoroscopic images, which record the knee postural changes during the activity. The registration of each bone segment is achieved by adjusting the motion parameters with respect to the joint-constraint model, making a simulated radiograph (SR) of the bone segment best matched to the underlying fluoroscopic image. Consequently, the registered knee postures in the entire fluoroscopic image sequence serve as the reconstruction result of 3-D knee motion.

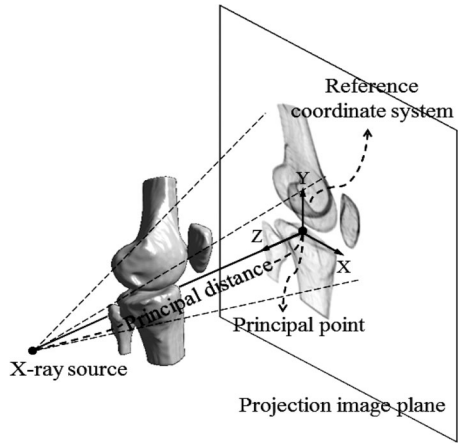

Fig. 1. Perspective viewing projection in single-plane fluoroscopy.

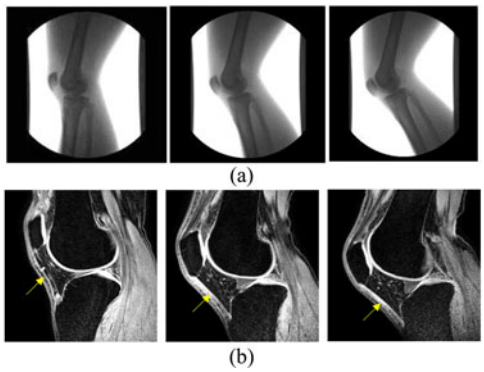

Fig. 2. (a) Example frames of fluoroscopic images during knee flexion, (b) example frames of MR volumetric images in postures 1, 2, and 3, respectively.

B. Estimation of Projection Parameters of Fluoroscopy

The projection parameters of fluoroscopy, which include both the principal point and principal istandce, can be used to reconstruct the geometry of an imaging system that is modeled using perspective viewing projection, as shown in Fig. 1. The principal point (i.e., the origin of the reference coordinate system) is the point on the image plane where the X-ray is incident perpendicularly, and the principal distance is the distance between the X-ray source and the principal point. Because X-ray images usually suffer from geometric distortion artifacts, we first use a third-order polynomial approximation approach [18] to correct the acquired images. After the image correction, we adopt a double-plate calibration setting to obtain the values of the principal distance and principal point based on the spatial relationship between 3-D points and their 2-D projections [7], [19].

C. Image Preparation

Single-plane fluoroscopy was used to record the projection details of knee motion. In order to acquire the knee fluoroscopic images, the subject was asked to lie on the platform of the fluoroscopy scanner (Toshiba ADR-1000A) and to flex the knee at a comfortable speed. The X-ray was emitted along the medial-lateral direction, and example frames of the acquired fluoroscopic images are shown in Fig. 2(a). The frame rate of video fluoroscopy was 10 frames/s, and the pixel size was 0.37 mm $\times$ 0.37 mm. On the other hand, to obtain a detailed 3-D knee structure, we acquired three postural MR images at knee bending degrees of 0, 30, and 60 by using a Philips 1.5 T Achieva system. The three postural images are denoted as postures 1, 2, and 3, respectively, and example frames are shown in Fig. 2(b). The slicing planes for the three postures were the sagittal plane (slicing thickness: 3 mm; spacing between slices: 1.5 mm). The imaging protocol we adopted was a 3-D gradient echo sequence repetition time of 20 ms, an echo time of 7.5 ms, and a flip angle of 50°. The pixel size was 0.3125 mm $\times$ 0. 3125 mm.

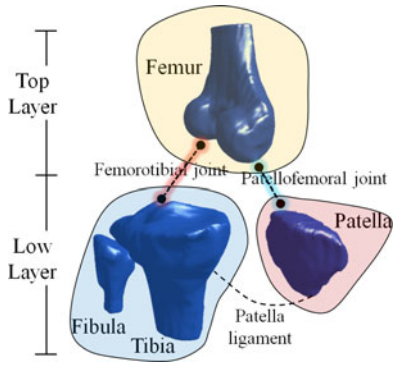

Fig. 3. Overview of the knee joint constraint model including surfaces and joint articulations.

D. Construction of the Knee Joint-Constraint Model

1) Model Architecture: The knee model used to control the articulated motion of knee bone segments plays a pivotal role in the proposed model-based registration. The knee model consists of four bone segments including the femur, tibia, fibula, and patella, and the volumes of bone segments are extracted semiautomatically from the MR image of posture 1 using the livewire approach [20]. The bone surfaces are triangulated using the marching cube algorithm [21] and then smoothed to remove local fluctuations.

As the human knee is an articulated structure, which does not allow the knee bone segments to move individually, we hence assign the knee model a hierarchical relationship to specify the order of bone registration and articulated transformation. Since the relative movement between the tibia and fibula is tiny, they are grouped as one component. Fig. 3 shows an overview of the model architecture. The femur on the top layer determines the global knee motion, while the other two components on the lower layer are capable of performing relative motion to the femur. Moreover, the tibia component has more shape features compared to the patella, it would be easier to first register the tibia with the fluoroscopic image. After the tibia is well registered, an anatomical constraint of the patellar ligament is employed to estimate the posture of the patella more reliably. The geometric transformations of the bone segments propagate from the top to low layers (following the order of femur, tibia and patella). Thus, the articulated relationships of the three bone components are able to be characterized in the knee model.

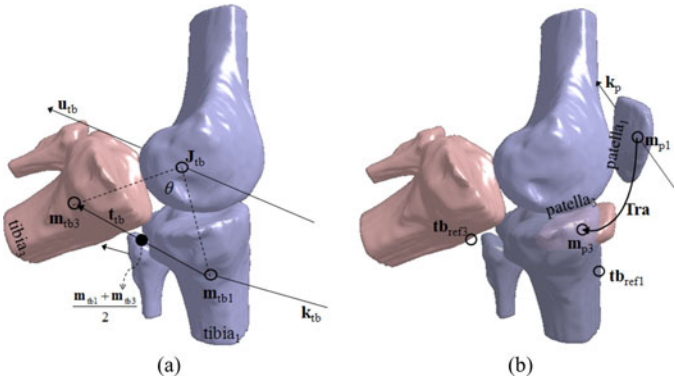

Fig. 4. Illustrations of (a) femorotibial and (b) patellofemoral joint parameter estimation.

On the other hand, in order to facilitate an understanding of joint functions and an assessment of the ranges of motion, the knee model has to represent all relevant bone points in their natural dimensions, the so-called anatomical coordinate systems. The anatomical coordinate systems are defined based on the biomechanics literatures [5], [22]. The x-axes of the femur, tibia, and patella coordinate systems are all parallel to the transepicondylar line. The y-axes of the three bone segments are determined by their respective longitudinal axes, and their z-axes are regarded as the outer product of the x- and y-axes.

2) Joint Mechanism: Generally, knee motion depends on the integrated movements of the knee bone segments constrained by the joint mechanism. There are two joints in the knee structure; one is the femorotibial joint, which determines the movement of tibia with respect to the femur, and the other is the patellofemoral joint, which controls the movement of patella with respect to the femur. To estimate the joint parameters of a given subject, at least two known postures are required for the purpose of analyzing the joint motion. By using our previously developed registration-based segmentation method [17], the knee bones in postures 2 and 3 can be automatically segmented. The geometric transformations, determining the relative motion of knee bones between different postures, can be obtained from the segmentation step for the purpose of deriving the femorotibial and patellofemoral joint parameters.

a) Femorotibial joint: The femorotibial joint acts as a modified hinge joint with a bicondylar structure (i.e., the pair of round bony protrusions in the medial and lateral sides of bottom of the femur). It can afford a combination of motions, including flexion/extension, rolling, and slight sliding [23]. The proposed method uses the joint parameters, including two centers of rotation (COR), two axes of rotation (AOR) and a plane of translation, to simulate the femorotibial joint mechanism. Note that the rotation angles and displacements with respect to the joint parameters are called motion parameters. As exemplified in Fig. 4(a), the tibia moves with respect to the femur from posture 1 to posture 3. The transformation matrix, which describes the movement of the tibia from posture 1 to posture 3, is decomposed into a rotation matrix $\mathbf{R}_{\mathrm{tb}} = [r_{11}\ r_{21}\ r_{31}]^T [r_{12}\ r_{22}\ r_{32}]^T [r_{13}\ r_{23}\ r_{33}]^T$ and a translation vector $\mathbf{t}_{\mathrm{tb}}$. The tibia in the two postures are denoted as tibia_1 and tibia_3, respectively, and their centers of mass (COMs) are represented with $\mathbf{m}_{\mathrm{tb1}}$ and $\mathbf{m}_{\mathrm{tb3}}$, respectively. The relative motion of the tibia can hence be approximated by using a combination of geometric transformations, including the rotation around the AOR $\mathbf{k}_{\mathrm{tb}}$ located at the COR $\mathbf{m}_{\mathrm{tb1}}$, the rotation around the AOR $\mathbf{u}_{\mathrm{tb}}$ located at the COR $\mathbf{J}_{\mathrm{tb}}$, and the translation on the plane formed by points $\mathbf{J}_{\mathrm{tb}}$, $\mathbf{m}_{\mathrm{tb1}}$ and $\mathbf{m}_{\mathrm{tb3}}$.

Because the rotational motion is the major component of knee joint motion, we can assume that the motion from tibia_1 to tibia_3 contains pure rotations in order to simplify the derivation of the joint parameters. Given the rotation matrix $\mathbf{R}_{\mathrm{tb}}$, we can first retrieve $\mathbf{k}_{\mathrm{tb}}$ based on the Euler's rotation theorem:

$$\mathbf{k}_{\mathrm{tb}} = \frac{1}{2\sin\left(\arccos\left(\frac{r_{11}+r_{22}+r_{33}-1}{2}\right)\right)} \begin{bmatrix} r_{32}-r_{23} \\ r_{13}-r_{31} \\ r_{21}-r_{12} \end{bmatrix}. \quad (1)$$

Moreover, with the assumption of the pure rotational motion, the COR $\mathbf{J}_{\mathrm{tb}}$ can be calculated based on the isosceles triangle $\mathbf{J}_{\mathrm{tb}}\mathbf{m}_{\mathrm{tb1}}\mathbf{m}_{\mathrm{tb3}}$:

$$\mathbf{J}_{\mathrm{tb}} = \frac{\mathbf{m}_{\mathrm{tb1}} + \mathbf{m}_{\mathrm{tb3}}}{2} + \frac{\mathbf{k}_{\mathrm{tb}} \times \mathbf{t}_{\mathrm{tb}}}{\|\mathbf{k}_{\mathrm{tb}} \times \boldsymbol{t}_{\mathrm{tb}}\|} \left(\frac{\frac{\|\mathbf{t}_{\mathrm{tb}}\|}{2}}{\tan(\frac{\theta}{2})} \right) \quad (2)$$

where $\mathbf{t}_{\mathrm{tb}} = \mathbf{m}_{\mathrm{tb1}} - \mathbf{m}_{\mathrm{tb3}}$. Axis $\mathbf{u}_{\mathrm{tb}}$ can also be given by

$$\mathbf{u}_{\mathrm{tb}} = [\mathbf{m}_{\mathrm{tb1}} - \mathbf{J}_{\mathrm{tb}}] \times [\mathbf{m}_{\mathrm{tb3}} - \mathbf{J}_{\mathrm{tb}}]. \quad (3)$$

Consequently, using (1)–(3), all the joint parameters of the femorotibial joint can be estimated.

The tibia movements contain not only the flexion/extension rotation, but also the adduction/abduction and internal/external rotations, more or less. Thus, both the two rotation axes are used to simulate the tibia motion more realistically. On the other hand, there may be small variations from the assumption of the rotational motion because the tibia is physically allowed to slide slightly. To handle such variations, the model further affords translational motion along the plane through $\mathbf{J}_{\mathrm{tb}}$, $\mathbf{m}_{\mathrm{tb1}}$, and $\mathbf{m}_{\mathrm{tb3}}$. With the femorotibial joint parameters, the 3-D posture of the tibia can be represented by

$$\overline{\mathbf{Tb}} = \mathbf{R}_{\theta_{\mathrm{ktb}},\mathbf{k}_{\mathrm{tb}}} \mathbf{Tb} + \mathbf{R}_{\theta_{\mathrm{utb}},\mathbf{u}_{\mathrm{tb}}} \mathbf{m}_{\mathrm{tb}} + \mathbf{T}_{\mathrm{tb\_}x,\mathrm{tb\_}y} \quad (4)$$

where $\mathbf{Tb}$ and $\overline{\mathbf{Tb}}$ represent the 3-D coordinates of the tibia points in the knee model with respect to the tibia coordinate and reference coordinate systems, respectively. $\mathbf{R}_{\theta_{\mathrm{ktb}},\mathbf{k}_{\mathrm{tb}}}$ and $\mathbf{R}_{\theta_{\mathrm{utb}},\mathbf{u}_{\mathrm{tb}}}$ represent the rotation matrices given by rotation angles θ_{ktb} and θ_{utb}, with respect to AORs $\mathbf{k}_{\mathrm{tb}}$ and $\mathbf{u}_{\mathrm{tb}}$. $\mathbf{T}_{\mathrm{tb\_}x,\mathrm{tb\_}y}$ indicates the translation vector with two small displacements $t_{\mathrm{tb\_}x}$ and $t_{\mathrm{tb\_}y}$, which are constrained by the plane formed by points $\mathbf{J}_{\mathrm{tb}}$, $\mathbf{m}_{\mathrm{tb1}}$, and $\mathbf{m}_{\mathrm{tb2}}$. By giving the motion parameters $\theta_{\mathrm{ktb}}, \theta_{\mathrm{utb}}, t_{\mathrm{tb\_}x}$, and $t_{\mathrm{tb\_}y}$, we can consequently determine a proper posture for the tibia based on the femorotibial joint mechanism.

b) Patellofemoral joint: The motion of the patella with respect to the femur is controlled by the patellofemoral joint mechanism. There is a strong, flat fibrous band called the patellar ligament that adjoins the margins of the patella to the tuberosity of the tibia, as indicated by the arrow in Fig. 2(b). While the tibia flexes, the patellar ligament will simultaneously lead the patella

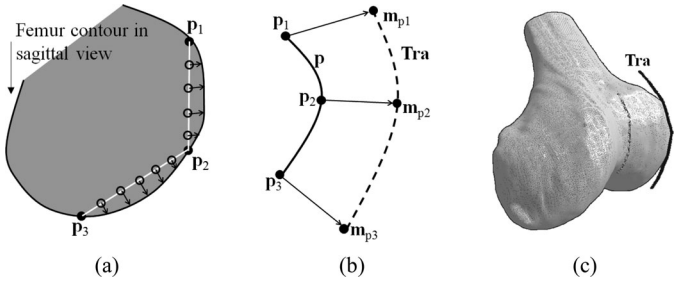

Fig. 5. Trajectory estimation for patella sliding: (a) projection of centers of mass of patellae on the femurs shown on a 2-D projection of femur, (b) trajectory interpolation, and (c) display of the trajectory.

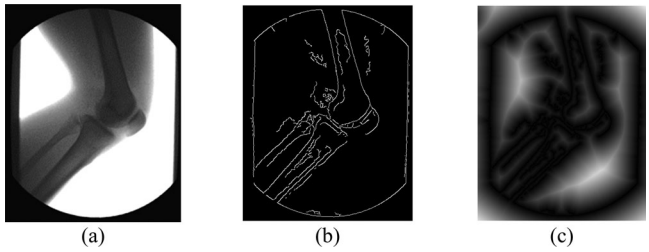

Fig. 6. Fluoroscopic image processing: (a) original fluoroscopic image, (b) edge map of (a) using canny edge detector, (c) distance field image of (b) using distance transform.

to slide along the femoral trochlear groove to avoid excessive stretching. To characterize such a motion in the proposed knee model, we use the joint parameters, including a COR, an AOR, and a translation trajectory, to simulate the patellofemoral joint mechanism.

The motion of the patella with respect to the femur between posture 1 and posture 3 is shown in Fig. 4(b). The patellae in the two postures are denoted as patella$_1$ and patella$_3$, respectively, and their COMs are represented with $\mathbf{m}_{\mathrm{p}1}$ and $\mathbf{m}_{\mathrm{p}3}$, respectively. $\mathbf{Tb}_{\mathrm{ref}1}$ and $\mathbf{Tb}_{\mathrm{ref}3}$ represent the positions of tibia tuberosity in postures 1 and 3, respectively. The motion of the patella can be characterized by the rotation around the AOR $\mathbf{k}_{\mathrm{p}}$ located at the COR $\mathbf{m}_{\mathrm{p}1}$, and the translation along trajectory **Tra**.

The AOR $\mathbf{k}_{\mathrm{p}}$ can be estimated using (1), while the trajectory **Tra** can be derived based on the spatial relationship between patella and femoral trochlear groove in different postures. To obtain a better approximation of the trajectory, three postures of the patella are utilized here. We first project the COM of the patella in the three postures along its posterior direction (z-axis of patella coordinate) onto the femur surface. The projection points are denoted as $\mathbf{p}_1$, $\mathbf{p}_2$, and $\mathbf{p}_3$, respectively, as indicated in Fig. 5(a). Then, we uniformly sample several points on the two line segments linking the three projection points, and move the lines to fit the closest curve on the femur surface of the knee model, as indicated by the solid curve $\mathbf{p}$ in Fig. 5(b). The curve $\mathbf{p}$ is located in the plane through the three points $\mathbf{p}_1$, $\mathbf{p}_2$, and $\mathbf{p}_3$ which are the projected positions of the three COMs $\mathbf{m}_{\mathrm{p}1}$, $\mathbf{m}_{\mathrm{p}2}$, and $\mathbf{m}_{\mathrm{p}3}$. Moreover, it is with dense points via B-spline interpolation. Next, $\mathbf{p}_1$, $\mathbf{p}_2$, and $\mathbf{p}_3$ on the curve are aligned back to $\mathbf{m}_{\mathrm{p}1}$, $\mathbf{m}_{\mathrm{p}2}$, and $\mathbf{m}_{\mathrm{p}3}$, respectively. The trajectory **Tra** is then parameterized based on the sum of the weighted shifts in $\mathbf{p}_1$, $\mathbf{p}_2$, and $\mathbf{p}_3$ to better match the shape of the femur trochlear groove:

$$\mathbf{Tra}(s) = \begin{cases} \mathbf{p}(s) + w_{1,2}(s)(\mathbf{m}_{\mathrm{p}1} - \mathbf{p}_1) + (1 - w_{1,2}(s))(\mathbf{m}_{\mathrm{p}2} - \mathbf{p}_2), s \in [1,2] \\ \mathbf{p}(s) + w_{2,3}(s)(\mathbf{m}_{\mathrm{p}2} - \mathbf{p}_2) + (1 - w_{2,3}(s))(\mathbf{m}_{\mathrm{p}3} - \mathbf{p}_3), s \in (2,3] \end{cases} \tag{5}$$

where $\mathbf{p}(s)$ represents a point on the curve $\mathbf{p}$, and $w_{1,2}(s)$ and $w_{2,3}(s)$ are the weighting values, inversely proportional to the distances between $\mathbf{p}(s)$ and $\mathbf{p}_1$ and between $\mathbf{p}(s)$ and $\mathbf{p}_2$, respectively. The obtained trajectory **Tra** for patella sliding is demonstrated in Fig. 5(c).

Given the patellofemoral joint parameters, the 3-D posture of patella can be represented by $\overline{\mathbf{P}}$:

$$\overline{\mathbf{P}} = \overline{\mathbf{m}}_{\mathrm{p}} + \mathbf{R}_{\theta_{\mathrm{p}},\mathbf{k}_{\mathrm{p}}}\mathbf{P} + \mathbf{T}_{\mathrm{p}\_x,\mathrm{p}\_y} \tag{6}$$

$$\overline{\mathbf{m}}_{\mathrm{p}} = \mathbf{Tra}(s), \text{subject to } \left\|\mathbf{Tra}(s) - \overline{\mathbf{tb}}_{\mathrm{ref}}\right\| = \left\|\mathbf{m}_{\mathrm{p}} - \mathbf{tb}_{\mathrm{ref}}\right\| \tag{7}$$

where $\mathbf{P}$ and $\overline{\mathbf{P}}$ represent the 3-D coordinates of patella points of the knee model with respect to the patella coordinate and reference coordinate systems, respectively. $\mathbf{m}_{\mathrm{p}}$ and $\overline{\mathbf{m}}_{\mathrm{p}}$ represent the COMs of the patella before and after the tibia moves, respectively. $\mathbf{tb}_{\mathrm{ref}}$ and $\overline{\mathbf{tb}}_{\mathrm{ref}}$ are the 3-D coordinates of the tuberosity point of the tibia before and after movements, respectively. $\mathbf{R}_{\theta_{\mathrm{p}},\mathbf{k}_{\mathrm{p}}}$ indicates the rotation matrix given by rotation angle θ_{p} and the AOR $\mathbf{k}_{\mathrm{p}}$. $\mathbf{T}_{\mathrm{p}\_x,\mathrm{p}\_y}$ is the translation vector with two small displacements t_{p_x} and t_{p_y} constrained by the plane containing the patella slide trajectory. By giving the values of the motion parameters θ_{p}, t_{p_x} and t_{p_y}, a 3-D posture of the patella can be determined using (6).

As these joint parameters are directly estimated based on the multipostural MR images, the resulting parameters can better match the joint motion patterns of the given subject. For each subject, the joint parameters are automatically determined based on the multipostural MR images before the model-based registration step (see Section II-F). The subject-specific joint model can then be used to adjust the knee posture to match different frames in the fluoroscopic image sequence, or even images from different acquisitions of the same subject.

E. Fluoroscopic Image Processing

In order to extract the image features for the registration process, several image processing techniques are sequentially implemented on the fluoroscopic images. First, a contrast-limited adaptive histogram equalization approach [24] is used to enhance image contrast, and then the anisotropic diffusion smoothing filter [25] is employed to remove image noises. Next, using the canny edge detector, we can obtain a set of edge maps of the fluoroscopic images [26]. By applying the distance transform [26] to each edge map, we can generate a distance field image (DFI), whose intensity is directly proportional to the distance of the pixel to its nearest edge point. Fig. 6 shows the intermediate results for the fluoroscopic image processing step. The resulting DFIs, which not only specify the presence/absence

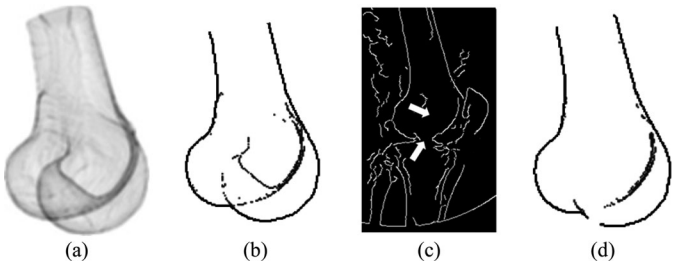

Fig. 7. SR generation and processing: (a) an example of the SR, (b) the corresponding $\mathrm{SR_{em}}$ of (a), (c) bone borders in a fluoroscopic image, and (d) $\mathrm{SR_{em}}$ after noncorresponding point removal.

of edge points but also embed a cost at each pixel of the fluoroscopic image, are used in the following model-based registration process.

F. Model-Based Image Registration

In the proposed model-based registration, a hierarchical framework is designed to register the bone segments of the knee model to each frame of the given video fluoroscopy image. For each bone segment, the 2-D–3-D registration is achieved by using an iterative optimization algorithm. At first, the 3-D posture of the bone segment is adjusted according to its corresponding joint parameters. Then, an SR is generated for the posture-adjusted bone segment. The similarity between the SR and fluoroscopic image is subsequently evaluated based on an edge-based fitness measure. The iterative process is regarded as converged until the fitness value is maximized. The geometric transformation determining the relative motion of the bone segment can be estimated and then propagated according to the bone hierarchy. After all the bone segments are registered, the 3-D posture of the knee model best matched to the current fluoroscopic frame can be readily obtained, and used as the initial guess of the knee posture in the next frame. Therefore, the knee moving postures recorded in the entire fluoroscopic image sequence, with the exception of the first frame, can then be identified automatically. As to the first frame, we can manually adjust the parameters to give a reasonable initial posture, and then optimize it using the proposed registration method.

1) Generation of the SR: The SR, a synthetic X-ray image of a 3-D object, is generated by simulating the X-ray attenuation in the imaging process. Given the initial posture of a bone segment from the knee model, we project the points of the bone segment onto the *x*–*y* plane of the reference coordinate system, and the coordinates of the projection points are calculated by $(x_i', y_i') = (x_i \cdot f/(f - z_i), y_i \cdot f/(f - z_i))$, where f is the principal distance, and (x_i, y_i, z_i) represents the 3-D coordinate of the ith point of the bone segment with respect to the reference coordinate system. Considering the fact X-ray image intensities are determined based on the attenuation degree of X-rays detected by the film, we characterize the distribution of X-ray attenuation based on a 2-D map of summation of projection points. First, the number of bone points on the line from the X-ray source to each pixel of the SR is recorded. Then, by normalizing the histogram values to the interval [0, 255], we can obtain the SR [see Fig. 7(a)].

Algorithm 1: 2D-3D bone registration using the chamfer matching with non-corresponding point removal

1. Adjust the bone posture based on the corresponding joint parameters.
2. Generate an SR of the bone segment.
3. Construct the edge map $\mathrm{SR_{em}}$.
4. Calculate the distance value $DF(\mathbf{x})$ for each point $\mathbf{x}$ of the $\mathrm{SR_{em}}$.
5. Build the cumulative distribution function, *cdf*, for the calculated distance values.
6. Choose a threshold K:
   If $DF(\mathbf{x})$ is less than K, the point $\mathbf{x}$ is preserved;
   Otherwise, it is removed from $\mathrm{SR_{em}}$.
   The threshold K has to satisfy the premise that $cdf(K)$ is larger than a certain proportion of preserved edge points to the total points in the $\mathrm{SR_{em}}$.
7. Calculate the value of *Fit* between the thresholded $\mathrm{SR_{em}}$ and DFI using Eq. (8).
8. If not converged, return to step 1 (Convergence is determined if the value of *Fit* is maximized).

2) Chamfer Matching with Noncorresponding Point Removal: We present an edge-based matching algorithm for the 3-D posture of the knee bone model and the underlying fluoroscopic image. For the sake of extracting the bone edge information from the SR, first, an edge map ($\mathrm{SR_{em}}$) is constructed by retaining the border points between the bone region and the background and by preserving the inner points with intensity smaller than 150 [see Fig. 7(b)]. Ideally, given an optimal posture for a knee bone segment, the edge points on the $\mathrm{SR_{em}}$ should perfectly match the zero-grayscale pixels of the DFI from the fluoroscopic image. The fitness measure *Fit* is hence designed based on the chamfer distance error [27]:

$$Fit = \frac{1}{\sqrt{\frac{1}{N}\sum_{i=1}^{N} DF(\mathbf{c}_i)^2 + 1}} \tag{8}$$

where $\mathbf{c}_i$ is the coordinate of the ith edge points in the $\mathrm{SR_{em}}$, N is the number of edge points in the $\mathrm{SR_{em}}$, and $DF(\mathbf{c}_i)$ indicates its corresponding distance value in the DFI. The optimal posture of the processed bone segment can be estimated by solving the corresponding motion parameters that maximize (8) based on the Powell's multidimensional direction set method [28].

However, due to uneven X-ray absorption in the processed anatomical structures, the bone borders extracted from the fluoroscopic images are usually less complete and more disordered than those in the $\mathrm{SR_{em}}$, as can be seen in the comparisons shown between Fig. 7(b) and (c) (see the condyle edges). Such improper correspondence of edge points between the $\mathrm{SR_{em}}$ and fluoroscopic image is likely to cause unsatisfactory registration results. To handle this issue, we modify the matching algorithm by incorporating the noncorresponding point removal scheme (see Algorithm 1).

In the following experiments, the proportion values in the sixth step of Algorithm 1 were empirically assigned as 0.85, 0.7, and 0.8 for the femur, tibia, and patella, respectively. Fig. 7(d)

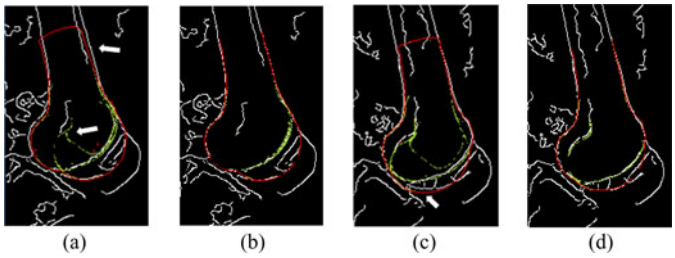

Fig. 8. Two registration results using (a) and (c) pure chamfer matching and (b) and (d) the proposed method. The red and green contours represent the outer and inner contours of the femur projection (SR_{em}), respectively. The white contours indicate the canny edge map of the fluoroscopic image.

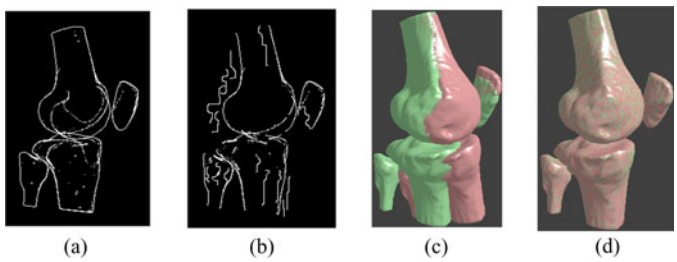

Fig. 9. Computer simulation experiment: (a) the computer simulated edge map, (b) the computer simulated edge map after manual modification, (c) and (d) superposition of the initial-given model (pink) and the ground truth (green) before and after the 2-D–3-D registration, respectively.

shows an example of SR_{em} after removing noncorresponding points. It can be seen that the resulting SR_{em} is better matched to the bone borders in the fluoroscopic image. Fig. 8 shows two examples for qualitative comparison between pure chamfer matching and the proposed method. It is found that if all the edge points in SR_{em} participate in the matching process, the registration tends to be trapped by undesirable local solutions (indicated by arrows). In contrast, the proposed method can select the edge points by finding the adequate cut on the cumulative distribution function, thus achieving a better match between the SR and the actual fluoroscopic image.

As the proposed joint-constraint model embeds the 3-D motion constraints of the total knee from multipostural MR images, the spatial relationship between the knee bone segments can be properly maintained during the registration process. The insufficiency of depth information can thus be compensated, and correct registration results can be achieved.

G. Joint-Space Interpolation Between Knee Postures

Considering that the radiation dose increases with the frame rate of fluoroscopy [29], the frame rate is usually limited and therefore is deficient in regard to capturing each instant of knee motion. To provide clinicians with detailed dynamic information of knee bone geometries, we present a joint-space interpolation scheme to generate knee postures during activity more densely.

From the previous 2-D–3-D registration step, we can obtain a set of sequential but discontinuous moving knee postures, each of which is matched to a frame of the fluoroscopic image sequence. The interpolation between two adjacent knee postures is achieved by using the proposed knee joint mechanism:

$$\mathbf{V}_r^t = \left(\prod_{a=0}^{2-r} \mathbf{M}_{2-a}^t \right) \mathbf{V}_r^0 \tag{9}$$

where $t \in [0, 1]$ is the time index in the whole motion sequence. The source and target postures are specified with t equals to zero and one, respectively. $\mathbf{V}_r^t$ represents the surface of the bone segment of layer r ($r = 2$: femur, $r = 1$: tibia, and $r = 0$: patella) in the frame at time t, and $\mathbf{V}_r^0$ is the surface of the corresponding bone in the source posture. $\mathbf{M}_r^t$ is expressed as a combination of rotation and translation matrices indicating the joint motion of layer r between the source and target postures in the frame at time t. By using (9), we can automatically generate proper postures in the interpolating trajectory and also conveniently obtain smooth knee motion.

III. Experiments and Results

The following experiments consisted of three tests on computer simulation, animal cadaver, and *in vivo* human knee data, respectively. The computer simulation and the animal cadaver experiments were conducted to validate the stability and accuracy of the proposed method. Moreover, to show the applicability of the proposed method to human data, we applied our system on three *in vivo* knees for reconstructing and analyzing the motion patterns.

A. Computer Simulation

To validate the stability of the proposed method, we designed a computer simulation experiment to illustrate how well the proposed method can perform under various initial conditions. At first, the ground truth in this experiment was provided by a knee model with known posture. Based on the ground truth, we generated an SR_{em} to specify the projection details of the knee model. It was observed from real fluoroscopic images that partial edges of the condyle, tibia plateau, and patella are too fuzzy to be extracted, and several irregular noisy edges appear nearby the bone segment contours. To make the SR_{em} more compatible with a real one, we manually erased some bone borders (e.g., the condyle edges) and added fake edges as the effects of X-ray imaging artifacts. Fig. 9(a) and (b) shows the SR_{em} before and after the manual modification, respectively. As the manual modification for the SR_{em} was not performed randomly, and instead, it was done by referring to the boundary appearance of real fluoroscopic images, the objectivity of the manual modification for adding noises and complexity in simulated reconstruction should be acceptable. After that, the DFI of the modified SR_{em} was used as the input for the model-based registration.

Next, fifty postures were generated by random perturbation with respect to the ground truth, as different initial conditions for the registration. The posture perturbation for each bone segment was carried out within a specific range as stated in Table I. Starting from these initial postures, fifty registration results were obtained using the proposed method. One of the fifty registration results was demonstrated to quantitatively show the effectiveness of the proposed method. Fig. 9(c) and (d) shows

TABLE I
RANGES OF SIMULATED KNEE POSTURES FOR SETTING INITIAL CONDITIONS IN THE MODEL-BASED REGISTRATION

Joint motion	Femur	Tibia	Patella
Translation (voxel)	$\sqrt{t_{f\_x}^2+t_{f\_y}^2+t_{f\_z}^2}=10$	None	$\sqrt{t_{p\_x}^2+t_{p\_y}^2}=5$
Rotation (degree)	$\lvert\theta_{f\_x}\rvert+\lvert\theta_{f\_y}\rvert+\lvert\theta_{f\_z}\rvert=7$	$\theta_{utb}\in[-10,10]$ $\theta_{ktb}\in[-10,10]$	$\theta_{p}\in[-5,5]$

TABLE II
MEAN TARGET REGISTRATION ERRORS UNDER DIFFERENT INITIAL CONDITIONS

mTRE in mm (mean, SD)	Femur	Tibia	Patella	Mean
Before registration	(6.75, 0.14)	(8.97, 3.45)	(7.96, 3.34)	8.09
After registration	(1.10, 1.03)	(1.46, 1.19)	(1.38, 1.39)	1.37

the knee model with initial posture (pink) coupled with the ground truth (green) before and after the registration, respectively. It can be observed that even though the femur, tibia, and patella are initially far away from their true positions, each bone segment can be well fitted to the ground truth, since the joint-constraint model allows an efficient search for the registration solutions.

Beyond the qualitative evaluation, we also conducted quantitative assessment in the computer simulation experiment. Each of the fifty registration results was evaluated based on the mean target registration error (mTRE) [30], which is defined to measure the average surface distance between the registered model and the ground truth:

$$\text{mTRE}=\frac{1}{M}\sum_{i=1}^{M}\left\|\overline{K_i}-K_i\right\| \tag{10}$$

where $\overline{K_i}$ and K_i represent the ith point of the ground truth and the registered knee model, respectively. M is the number of surface points in the knee model (femur: 77739; tibia (with fibula): 73123; patella: 16495). Table II shows the mean and standard deviation (SD) for the mTREs of each bone segment under the fifty initial conditions.

B. Animal Cadaver

An animal cadaveric experiment was conducted to validate the accuracy of the proposed method. Since the structure of lamb knee is similar to that of human, a lamb cadaveric knee was selected as the material for this experiment. At first, we cut off the knee from the hind leg of a lamb cadaver, including the femur, tibia, patella, and soft tissues (e.g., muscles and ligaments) around the knee joint. Then, we implanted 11 metallic markers with radius of 2.25 mm on the bone surfaces (four on the femur, four on the tibia, and three on the patella). The knee was subsequently placed and fixed on a self-made support to acquire three different postural volumetric images for the purpose of constructing the knee joint-constraint model. The posture of the cadaveric knee could be adjusted by changing the bending angle of the support [see Fig. 10(a)]. In order to obtain the signals for the metallic markers which are prohibited in MR imaging, a CT device (Siemens Sensation 16) was utilized in this experiment. Fig. 10(b) shows the reconstructed surfaces of the cadaveric knee model and metallic markers. In addition, a continuous motion sequence for the cadaver knee was recorded using single-plane video fluoroscopy in 186 frames. For the purpose of accuracy validation, we applied the proposed registration system to reconstruct the cadaveric knee motion.

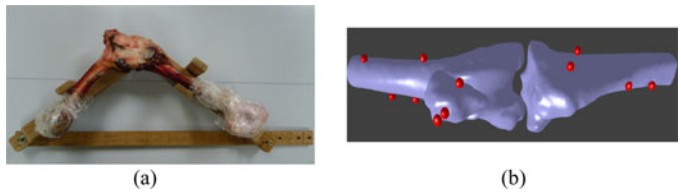

Fig. 10. Lamb cadaveric experiment: (a) the lamb cadaveric knee and the bone-attached metallic markers and (b) the reconstructed surfaces of cadaveric femur, tibia, patella, and markers.

TABLE III
DIFFERENCES IN THE GROUND-TRUTH TRANSFORMATION AND OUR REGISTRATION RESULTS (IN TERMS OF DISPLACEMENTS AND ROTATION ANGLES WITH RESPECT TO THE REFERENCE COORDINATE SYSTEM)

Difference of displacement in mm (mean, SD)	Along x-axis	Along y-axis	Along z-axis
Femur	(0.52, 0.35)	(0.17, 0.16)	(0.12, 0.13)
Tibia	(0.58, 0.32)	(0.45, 0.27)	(0.74, 0.37)
Patella	(0.45, 0.30)	(0.47, 0.43)	(0.37, 0.32)
Difference of rotation angle in degree (mean, SD)	**Around x-axis**	**Around y-axis**	**Around z-axis**
Femur	(0.09, 0.12)	(0.61, 0.63)	(1.70, 0.36)
Tibia	(0.41, 0.29)	(2.83, 0.28)	(1.17, 0.63)
Patella	(2.25, 1.89)	(1.20, 0.95)	(1.48, 0.53)

Since the markers are attached directly onto the surfaces of bone segments, the positions of the markers are able to determine the actual bone motion. Moreover, the markers on the fluoroscopic images present sharp and clear boundary appearances. Therefore, the ground-truth transformation of each bone segment can be accurately obtained by registering its corresponding markers to the underlying fluoroscopic image [16]. To ensure the accuracy of the ground truth, the marker registration result of each frame was further confirmed by an expert. The registration errors were evaluated by the difference between the ground-truth transformation and the one obtained by the proposed method [30], [31]. To facilitate the evaluation, we also decomposed the 3-D rigid transformation into three displacements along the three axes of the reference coordinate system, and three rotation angles around the three axes of reference coordinate system. For each of the six parameters, the average difference of the 186 frames is listed in Table III. Other than that, we also applied the two transformations to each bone segment of the knee model for assessing the mTRE. The mTREs of the 186 image frames for the femur, tibia, and patella were 1.15 ± 0.24, 1.48 ± 0.2, 0.75 ± 0.3 mm, respectively.

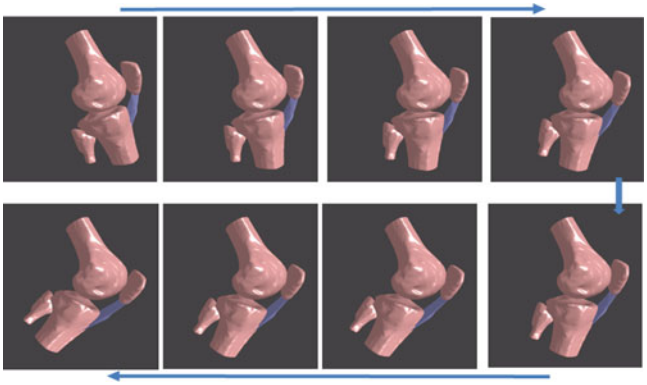

Fig. 11. Visualization of reconstructed *in vivo* knee motion with eight sequentially moving postures.

C. In Vivo Human Knees

In this experiment, we reconstructed three *in vivo* human knee motion using the proposed registration system, and accounted for the motion using both qualitative and quantitative observations. Two males and one female (twenty-four, twenty-five, and thirty years-old, respectively), who had no history of knee disorders, gave informed consent to participate in this study. Three postural MR images with bending degrees 0, 30, and 60, and a video fluoroscopy image recording the knee flexion motion of each subject were acquired. After the 2-D–3-D registration, we utilized the proposed joint space interpolation approach to obtain knee moving postures more densely. Fig. 11 shows eight sequentially moving postures acquired during the reconstructed motion, by which the dynamic spatial configuration between the femur, tibia, and patella can be clearly visualized. In addition, we further incorporated the patellar ligament (in purple), whose surface was manually constructed from the MR images, to increase the level of completion of the demonstration. It can be seen that the patellar ligament is stretchable to flexibly maintain the patella height in the knee joint structure. We believe that such a visualization of dynamic knee geometry is beneficial for medical education and practice.

On the other hand, we analyzed the motion pattern of three *in vivo* knees by decomposing the registration transformations into 6-degree-of-freedom relative motion. More specifically, the relative motion, including three rotations (flexion/extension, adduction/adduction, and internal/external) and three translations (medial/lateral, posterior/anterior and proximal/distal), could be estimated based on the geometric transformations between the tibia and femur coordinate systems, and between patella and femur coordinate systems [22], [32]. Fig. 12 illustrates the reconstructed motion patterns of the three subjects, including rotational and translational motion of femorotibial and patellofemoral joints during knee flexion.

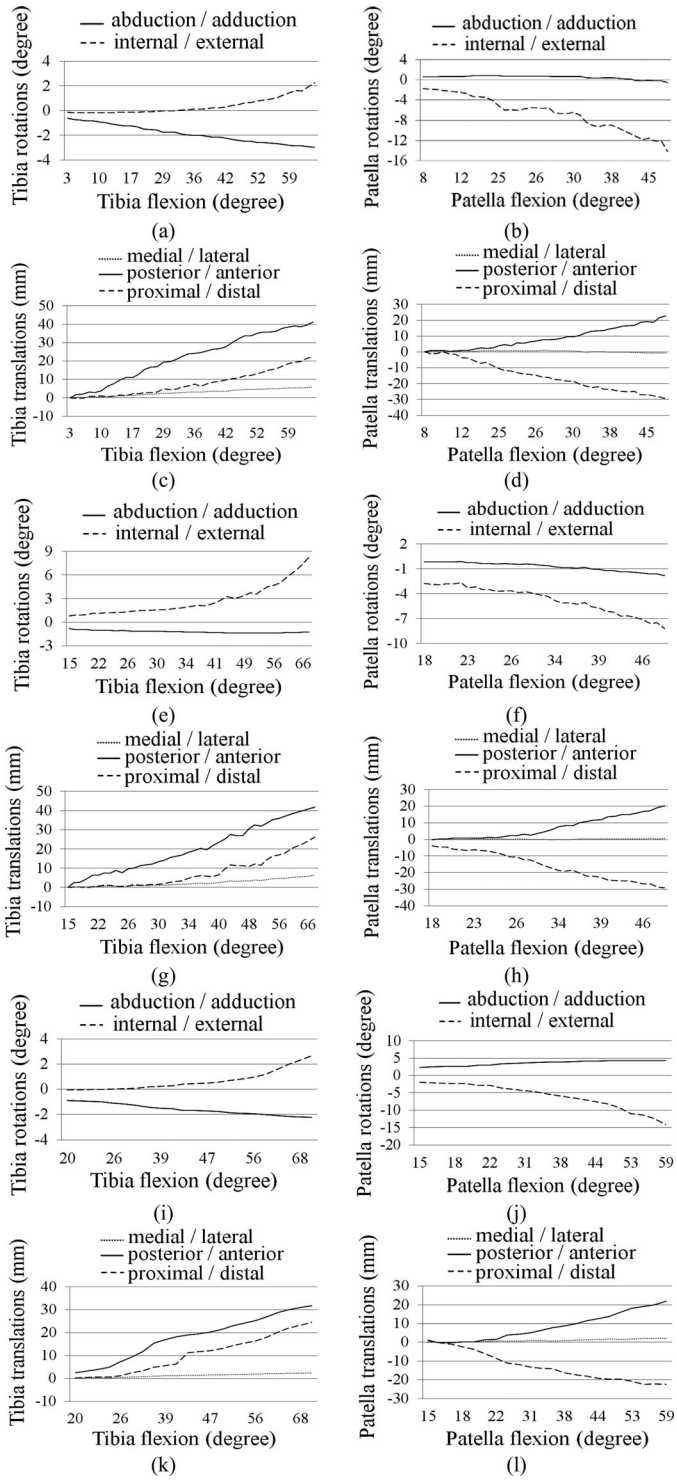

Fig. 12. Reconstruction of *in vivo* knee motion pattern; (a)–(d) subject 1, (e)–(h) subject 2, and (i)–(l) subject 3. For each subject, the four figures are sequentially shown as rotational motion in the femorotibial joint, rotational motion in the patellofemoral joint, translational motion in the femorotibial joint, and translational motion in the patellofemoral joint. The movement before the slash is with positive slope, and after the slash is with negative slope.

IV. Discussions

From the computer simulation experiment, it can be seen that the average mTRE after the registration was largely improved from 8.09 to 1.37 mm. The registration errors were small and acceptable in contrast with the criterion of 2 mm for a failed registration [30], [31]. In addition, the registration errors were also assessed based on a relative measure, which is the ratio of the mTRE to the actual length of a bone segment. The resulting error ratios for the femur, tibia, and patella were found to be

small, 1.13%, 2.02%, and 3.21%, respectively. As a whole, the stability of the proposed method was proven satisfactory in the computer simulation experiment.

In the animal cadaveric experiment, the average differences from the ground-truth transformation were less than 1 mm in errors presented in Fregly's work (around 5 mm for the femur and tibia/fibula and 10 mm for the patella) [9], ours (0.12 ± 0.13 mm for the femur, 0.74 ± 0.37 mm for the tibia, and 0.37 ± 0.32 mm for the patella) were relatively small and acceptable. The rotation error of the tibia around the y-axis was larger than those around the other two axes. It was probably because the lamb does not contain a fibula, which provides helpful edge information in determining the y-axis rotation of the tibia. This phenomenon also indicates that grouping the tibia and fibula as one bone component for edge-based 2-D–3-D registration (in human knees) could achieve a better estimation of tibia pose than registering the tibia individually. Moreover, the mTREs for the femur, tibia, and patella were 1.15 ± 0.24, 1.48 ± 0.2 and 0.75 ± 0.3 mm, respectively, which were considered successful according to the criterion of 2 mm [30], [31]. The registration errors, compared with the actual lengths of the cadaveric femur (39 mm), tibia (42 mm), and patella (20 mm), were also quite small.

As shown in Fig. 12 in the *in vivo* knee testing, the flexion of the femorotibial joint is coupled with the adduction and internal rotations. Such a phenomenon has been reported by Wilson *et al*. [33] on the motion analysis of human cadaveric knees. Yet, the coupled motions in our *in vivo* study are less than those in Wilson's study utilizing cadaver knees for motion analysis. The logical explanation of such a difference is because the joint constraints of *in vivo* knees supported by major soft tissues (e.g., muscle tension) and proprioceptive responses must be stronger than those of cadaver knees. Thus, the smaller adduction/adduction rotation observed in our results can be reasonably accounted for.

Fig. 12 also shows that the knee flexion to be coupled with obvious external and inconspicuous abduction/adduction rotations of patellofemoral joint. Such findings can also be physiologically explained from the anatomical point of view since the bicondylar structure of the femur certainly limits the range of abduction/adduction of the patella. Although the true kinematics of the *in vivo* knees were not available for validation, the sequences of the reconstructed motion showed reasonable physiologic patterns of motion. Consequently, the proposed system can demonstrate good applicability in reconstructing *in vivo* human knee motion.

Another merit of the proposed registration method is the efficiency of the time with regard to user interaction. To the best of our knowledge, in order to obtain a good registration, existing 2-D–3-D registration approaches require users to manually put the processed bone model close to the true position on each image frame. However, such a requirement is demanding when there are a large number of images contained in a motion sequence like the present study. Different from current methods, the proposed model-based method only needs this manual step done in the first frame and can accomplish the registration of the total knee in a fully automatic process for the rest of image frames. The computation time required for registering the whole dataset of one subject was assessed on a computer with an Intel Core i3–2310M processor (2.10 GHz) and 4.0 GB of memory. For the whole dataset of one subject (containing about 67 frames, and including 3 bone components in each frame), the total computation time was averagely in 75.05 min, and the average time for each frame was in 1.19 min. The computation cost can be further reduced by using a faster computer processor or a graphics processing unit (GPU)-based platform in the future.

The knee joint belongs to a condylar joint, which permits movements primarily in one plane; for example, the primary motion of the knee joint is flexion or extension in a sagittal plane, and other angular rotations and displacements were small [34], [35]. Moreover, the rocking motion of the patella is also approximately planar [35]. It can be reasonably inferred that the joint parameters such as AORs and CORs present limited variations from the ideal planar joint motion, and thus meet the aforementioned physical phenomena. The reproducibility of the joint models can thus be confirmed in some sense.

Although we did not have available diseased knees for the experiments in this paper, we will apply the model-based system to investigate the kinematics of pathological knee joints in the future. The concept of the proposed method was to approximate the 3-D femorotibial and patellofemoral joint models based on the multipostural MR images, and then to estimate the joint motion parameters using the reconstructed joint models from the corresponding sagittal fluoroscopic image sequence. If the observed pathological case does not involve any deformity of the joint structure, the proposed model is still capable of reconstructing the joint motion based on the coupling of 3-D reconstructed model and corresponding fluoroscopic image sequence. For instance, if the subject suffers from anterior cruciate ligament injury and the abnormal motion of knee joint can be shown in both MR and fluoroscopic images, the reconstructed motion model still can reflect the exact motion of the subject. Yet, the motion model might not be smooth if the observed pathological case involves deformity of joint structure, which could be a potential limitation of the present system.

V. Conclusion

We have proposed a new 2-D–3-D registration system, which combines the articulated joint models, kinematics properties, and image features, for reconstructing total knee motion using single-plane fluoroscopy. The joint models can properly characterize the solution space of 2-D–3-D registration, reducing the effects of insufficient information from the single-plane fluoroscopy on the accuracy of the motion reconstruction. Another notable feature of the proposed system is that the fluoroscopy-based patella tracking can be achieved though the image and shape features of the patella are not salient. We also presented the noncorresponding point removal scheme with the chamfer distance measure to successfully reduce the instability of edge matching in the 2-D–3-D registration.

Three experiments including computer simulation, animal cadaveric, and *in vivo* knee testing were conducted to validate

the effectiveness of the proposed method. We achieved satisfactory accuracy of registration for the femur, tibia, and patella with mTREs less than 1.5 mm. Moreover, the out-of-plane translation error, which is a common problem for conventional 2-D–3-D registration methods, was found to be small (less than 1 mm) using the proposed joint models. In the future, effort will be devoted to assessing the differences in motion patterns between healthy and diseased knees. We can also complete the knee model by including more anatomical tissues, so that the interaction between rigid and soft tissues during knee activity can be better demonstrated for evaluating the knee functionality.

REFERENCES

[1] T. Norimatsu, M. Osaki, M. Tomita, Z. Ye, Y. Abe, S. Honda, M. Kanagae, S. Mizukami, N. Takamura, Y. Kusano, H. Shindo, and K. Aoyagi, "Factors predicting health-related quality of life in knee osteoarthritis among community-dwelling women in Japan: The Hizen–Oshima study," *Orthopedics*, vol. 34, no. 9, pp. e535–e540, 2011.

[2] O. Bruyere, A. Honore, O. Ethgen, L. C. Rovati, G. Giacovelli, Y. E. Henrotin, L. Seidel, and J.-Y. L. Reginster, "Correlation between radiographic severity of knee osteoarthritis and future disease progression. Results from a 3-year prospective, placebo-controlled study evaluating the effect of glucosamine sulfate," *Osteoarthritis Cartilage*, vol. 11, pp. 1–5, 2003.

[3] J. X. Chen, H. Wechsler, P. J. Mark, Y. Zhu, and E. B. Macmahon, "Knee surgery assistance: Patient model construction, motion simulation, and biomechanical visualization," *IEEE Trans. Biomed. Eng.*, vol. 48, no. 9, pp. 1042–1052, Sep. 2001.

[4] C. J. Lin, J. S. Ho, Y. L. Chou, W. Huang, and S. C. Lin, "Physiological knock-knee in preschool children: Prevalence, correlating factors, gait analysis and clinical significance," *J. Pediatric Orthopaedics*, vol. 19, no. 5, pp. 650–654, 1999.

[5] F. Lin, M. Makhsous, A. H. Chang, R. W. Hendrix, and L. Q. Zhang, "*In vivo* and noninvasive six degrees of freedom patellar tracking during voluntary knee movement," *Clin. Biomech.*, vol. 18, pp. 401–409, 2003.

[6] D. L. Benoit, D. K. Ramsey, M. Lamontagne, L. Xu, P. Wretenberg, and P. Renstrom, "Effect of skin movement artifact on knee kinematics during gait and cutting motion measured *in vivo*," *Gait Posture*, vol. 24, no. 2, pp. 152–164, 2006.

[7] S. A. Banks and W. A. Hodge, "Accurate measurement of three-dimensional knee replacement kinematics using single-plane fluoroscopy," *IEEE Trans. Biomed. Eng.*, vol. 43, no. 6, pp. 638–649, Jun. 1996.

[8] S. Zuffi, A. Leardini, F. Catani, S. Fantozzi, and A. Cappello, "A model-based method for reconstruction of total knee replacement kinematics," *IEEE Trans. Med. Imag.*, vol. 18, no. 10, pp. 981–991, Oct. 1999.

[9] B. J. Fregly, H. A. Rahman, and S. A. Banks, "Theoretical accuracy of model-based shape matching for measuring natural knee kinematics with single-plane fluoroscopy," *J. Biomech. Eng.*, vol. 127, no. 4, pp. 692–699, 2005.

[10] T. Y. Tsai, T. W. Lu, C. M. Chen, M. Y. Kuo, and H. C. Hsu, "A volumetric model-based 2D to 3D registration method for measuring kinematics of natural knees with single-plane fluoroscopy," *Med. Phys.*, vol. 37, no. 3, pp. 1273–1284, 2010.

[11] G. P. Penney, P. G. Batchelor, D. L. G. Hill, D. J. Hawkes, and J. Weese, "Validation of a two- to three-dimensional registration algorithm for alignment preoperative CT images and intraoperative fluoroscopy images," *Med. Phys.*, vol. 28, no. 6, pp. 1024–1032, 2001.

[12] B. Ma, J. Stewart, D. Pichora, R. Ellis, and P. Abolmaesumi, "2-D/3-D registration of multiple bones," in *Proc. 29th IEEE Annu. Int. Conf. Eng. Med. Biol. Society*, Lyon, France, 2007, pp. 860–863.

[13] T. Yamazaki, T. Watanabe, Y. Nakajima, K. Sugamoto, T. Tomita, H. Yoshikawa, and S. Tamura, "Improvement of depth position in 2-D/3-D registration of knee implants using single-plane fluoroscopry," *IEEE Trans. Med. Imag.*, vol. 23, no. 5, pp. 602–612, May 2004.

[14] J. Laprade and R. Lee, "Real-time measurement of patellofemoral kinematics in asymptomatic subjects," *The Knee*, vol. 12, pp. 63–72, 2005.

[15] G. R. Waryasz and A. Y. McDermott, "Patellofemoral pain syndrome (PFPS): A systematic review of anatomy and potential risk factors," *Dyn. Med.*, vol. 7, pp. 9–22, 2008.

[16] T. S. Y. Tang, N. J. MacIntyre, H. S. Gill, R. A. Fellows, N. A. Hill, D. R. Wilson, and R. E. Ellis, "Accurate assessment of patellar tracking using fiducial and intensity-based fluoroscopic techniques," *Med. Image Anal.*, vol. 8, pp. 343–351, 2007.

[17] H. C. Chen, I. M. Jou, C. K. Wang, F. C. Su, and Y. N. Sun, "Registration-based segmentation with articulated model from multipostural magnetic resonance images for hand bone motion animation," *Med. Phys.*, vol. 37, no. 6, pp. 2670–2682, 2010.

[18] E. Gronenschild, "Correction for geometric image distortion in the x-ray imaging chain: Local technique versus global technique," *Med. Phys.*, vol. 26, no. 12, pp. 2602–2616, 1999.

[19] Th. Leloup, W. El Kazzi, O. Debeir, F. Schuind, and N. Warzée, "Automatic fluoroscopic image calibration for traumatology intervention guidance," in *Proc. Int. Conf. Comput. Tool* , 2005, pp. 374–377.

[20] J. Liu, J. K. Udupa, and P. K. Saha, "Rigid model-based 3D segmentation of the bones of joints in MR and CT images for motion analysis," *Med. Phys.*, vol. 35, no. 8, pp. 3637–3649, 2008.

[21] W. E. Lorensen and H. E. Cline, "Marching cubes: A high resolution 3-D surface construction algorithm," *Comput. Graph.*, vol. 21, no. 4, pp. 163–169, 1987.

[22] G. Wu and P. R. Cavanagh, "ISB recommendations for standardization in the reporting of kinematic data," *J. Biomech.*, vol. 28, no. 10, pp. 1257–1261, 1995.

[23] P. Komdeur, F. E. Pollo, and R. W. Jackson, "Dynamic knee motion in anterior cruciate impairment: a report and case study," *BUMC Proc.*, vol. 15, pp. 257–259, 2002.

[24] S. M. Pizer, E. P. Amburn, J. D. Austin, R. Cromartie, A. Geselowitz, T. Greer, B. H. Romeny, J. B. Zimmerman, and K. Zuiderveld, "Adaptive histogram equalization and its variations," *Comput. Vision., Graph., Image Process.*, vol. 39, pp. 355–368, Sep. 1987.

[25] G. Gerig, O. Kubler, R. Kikinis, and F. A. Jolesz, "Nonlinear anisotropic filtering of MRI data," *IEEE Trans. Med. Imag.*, vol. 11, no. 2, pp. 221–232, Jun. 1992.

[26] M. Sonka, V. Hlavac, and R. Boyle, *Image Processing, Analysis, and Machine Vision*, 3rd ed. Stamford, CT, USA: Thomson Learning, 2007.

[27] G. Borgefors, "Hierarchical chamfer matching: A parametric edge matching algorithm," *IEEE Trans. Pattern Anal. Mach. Intell.*, vol. 10, no. 6, pp. 849–865, Nov. 1988.

[28] W. H. Press, S. A. Teukolsky, W. T. Vetterling, and B. P. Flannery, *Numerical Recipes in C*, 2nd ed. Cambridge, MA, USA: Cambridge Univ. Press, 1992.

[29] H. D. Allen, D. J. Driscoll, R. E. Shaddy, and T. F. Feltes, *Moss and Adams' Heart Disease in Infants, Children and Adolescents: Including the Fetus and Young Adult*, 7th ed. Lippincott, PA, USA: Williams & Wilkins, 2008, p. 221, ch. 9.

[30] E. B. Van de Kraats, G. P. Penney, D. Tomaževič, T. van Walsum, and W. J. Niessen, "Standardized evaluation methodology for 2-D–3-D registration," *IEEE Trans. Med. Imag.*, vol. 24, no. 9, pp. 1177–1189, Sep. 2005.

[31] D. Tomaževič, B. Likar, T. Slivnik, and F. Pernuš, "3-D/2-D Registration of CT and MR to X-Ray Images," *IEEE Trans. Med. Imag.*, vol. 22, no. 11, pp. 1407–1416, Nov. 2003.

[32] G. K. Cole, B. M. Nigg, J. L. Ronsky, and M. R. Yeadon, "Application of the joint coordinate system to three-dimension joint attitude and movement representation: A standardization proposal," *J. Biomechanical Eng.*, vol. 115, pp. 344–349, 1993.

[33] D. R. Wilson, J. D. Feikes, A. B. Zavatsky, and J. J. O'Connor, "The components of passive knee movement are coupled to flexion angle," *J. Biomech.*, vol. 33, pp. 465–473, 2000.

[34] D. L. Bartel, D. T. Davy, and T. M. Keaveny, *Orthopaedic Biomechanics: Mechanics and Design in Musculoskeletal Systems*. Upper Saddle River, NJ, USA: Pearson, 2006.

[35] G. T. Yamaguchi and F. E. Zajac, "A planar model of the knee joint to characterize the knee extensor mechanism," *J. Biomech.*, vol. 22, no. 1, pp. 1–10, 1989.

Authors' photographs and biographies not available at the time of publication.